Journal of Rock Mechanics and Geotechnical Engineering 10 (2018) 778–790

Contents lists available at ScienceDirect

Journal of Rock Mechanics and Geotechnical Engineering

journal homepage: www.rockgeotech.org

Full Length Article

Revising the unified hardening model by using a smoothed Hvorslev envelope

Annan Zhou [a,*], Yangping Yao [b]

[a] School of Engineering, Royal Melbourne Institute of Technology (RMIT), Melbourne, VIC 3001, Australia
[b] Department of Civil Engineering, Beihang University, Beijing, 100191, China

ARTICLE INFO

Article history:
Received 3 August 2017
Received in revised form
8 October 2017
Accepted 23 October 2017
Available online 26 May 2018

Keywords:
Constitutive model
Clay
Overconsolidation
Hvorslev envelope
Hermite interpolation

ABSTRACT

The original unified hardening (UH) model, in which a straight Hvorslev envelope was employed to determine the potential peak stress ratio of overconsolidated soils, is revised using a smoothed Hvorslev envelope (Hermite-Hvorslev envelope). The strength at the intersection between the straight Hvorslev envelope and the critical state surface (i.e. Mohr-Coulomb envelope) can be undefined due to the discontinuous change in the slope of the two linear strength envelopes mentioned above. A smoothed Hvorslev envelope is derived through Hermite interpolation to ensure a smooth change between the proposed Hvorslev envelope and the zero-tension surface as well as a smoothed transition between the proposed Hvorslev envelope and the critical state surface. The Hermite-Hvorslev envelope is then integrated into the original UH model, and then the UH models with four different functions of the Hvorslev envelope are compared with each other. The UH model revised by the Hermite-Hvorslev envelope can well predict the mechanical behaviors of normally consolidated and overconsolidated soils in drained and undrained conditions with the same parameters in the modified Cam-Clay model.

1. Introduction

Most clays encountered in geotechnical engineering are subjected to a preconsolidation pressure higher than the current pressure and, therefore, are overconsolidated to some extent because of human activities (such as compaction, excavation, and tillage) and changes in the environmental loads (such as landsides, rainfall/evaporation, and fluctuations of groundwater level). Theoretically, although soils are separated into normally consolidated and overconsolidated soils, overconsolidated soils are more general because normally consolidated soil can be regarded as a special case of overconsolidated soil with an overconsolidation ratio (OCR) equal to one. Soil behaves differently because of the variation in the OCR value, which has been reported in many experimental results (Banerjee and Stipho, 1979; Nakai and Hinokio, 2004). Normally consolidated soil exhibits a monotonically increasing stress ratio that will approach a constant contractive volume change during shearing. On the other hand, overconsolidated soil with an OCR greater than one may exhibit a peak stress ratio and post-peak softening behavior subjected to shearing, both of which become more distinct with increasing OCR. In addition, compared with normally consolidated soil, overconsolidated soil may show a dilative volume change after volume contraction during shearing. The shearing related volume dilation can be more distinct due to the increase in the OCR value. In isotropic stress conditions, overconsolidated soil is less compressive (i.e. stiffer) compared with the normally consolidated soil with the identical initial stress, and the stiffness of the overconsolidated soil gradually increases with an increase in the OCR.

The modified Cam-Clay model is successful in modeling the mechanical behaviors of normally consolidated and lightly overconsolidated clays (usually the OCR is less than 2), such as the critical state and volume contraction caused by shearing. However, it is not suitable for reproducing the mechanical responses of medium or heavily overconsolidated clays, such as the peak strength, post-peak softening and shear-dilation. Therefore, based on the modified Cam-Clay model, a number of approaches have been proposed to interpret and simulate the typical mechanical behaviors of overconsolidated soils, especially to build a unified constitutive framework to describe the continuous behavior change of soils for the entire range of the OCR (from 1 to infinite). For example, Pender (1978) proposed a semi-empirical but practical

* Corresponding author.
E-mail address: annan.zhou@rmit.edu.au (A. Zhou).
Peer review under responsibility of Institute of Rock and Soil Mechanics, Chinese Academy of Sciences.

https://doi.org/10.1016/j.jrmge.2017.10.008

constitutive model for overconsolidated soils based on three hypotheses on the yield surface (f), potential surface (g) and hardening function (h), using experimental observations. Mrŏz et al. (1978) employed a set of nesting surfaces in the stress space in addition to the yield surface to specify the variation of the 'hardening moduli field', during the deformation process with complex loading programs involving loading, unloading and cycle loading. Based on the concept of nesting surfaces, Dafalias and Herrmann (1986) introduced the 'bounding surface plasticity' and then applied the radial mapping version of the bounding surface plasticity to modeling the mechanical behaviors of overconsolidated clayey soils. The bounding surface plasticity was also included in the MIT-E3 model (Whittle and Kavvadas, 1994) to reproduce the irrecoverable, anisotropic and path-dependent behavior of overconsolidated clays with an OCR less than eight. Ling et al. (2002) incorporated rotational and distortional hardening rules into the bounding surface formulation with an associated flow rule to predict the mechanical behavior of anisotropically overconsolidated clays. Morvan et al. (2010) extended bounding surface plasticity from saturated overconsolidated soils to unsaturated overconsolidated soils. On the other hand, based on the concept of nesting surfaces, Hashiguchi (1980) extended the concept of a yield surface to the sub-yield state under the distinct yield state and assumed the existence of a 'sub-loading surface' in the sub-yield state. Nakai and Hinokio (2004) developed a constitutive model based on the sub-loading surface plasticity to simulate the typical deformation and strength behavior of normally consolidated and isotropically overconsolidated clays in general stress conditions. Most recently, Zhou and Sheng (2015) developed a hydro-mechanical coupled constitutive model for unsaturated overconsolidated soils based on the sub-loading surface plasticity. However, most of these models have limited engineering applications due to the large number of model parameters. Some of these model parameters, as noted by Yao et al. (2012), are difficult to be calibrated through conventional laboratory tests, and their values can often only be determined by a trial-and-error method.

For engineering applications, Yao et al. (2008a, 2009) proposed a robust elastoplastic model to interpret the mechanical behaviors of both normally consolidated and overconsolidated soils based on the sub-loading surface concept, the straight Hvorslev envelope and the unified hardening (UH) parameter (Yao et al., 2007, 2008b). The proposed model, referred to as the original UH model, is simple and practical because it only includes one additional parameter (i.e. the Hvorslev slope) compared with the modified Cam-Clay model. Yao et al. (2012) replaced the original straight Hvorslev envelope by a parabolic one with an initial slope of less than 3 to avoid unrealistic implications in the original UH model because the zero-tension surface is not included. It was employed in developing time-dependent UH model (Yao et al., 2015). However, it is subjective to assume that the Hvorslev envelope must be expressed by an ad hoc parabolic function without justification. Therefore, Yao and Zhou (2013) used the piecewise Hvorslev envelope (i.e. a combination of the zero-tension line and the straight Hvorslev envelope) when they extended the original UH model from isothermal to non-isothermal conditions. However, with respect to all three UH models, the Hvorslev envelope (straight, parabolic and piecewise) cannot join into the critical state line (i.e. Mohr-Coulomb envelope) smoothly. In other words, the slope of the strength envelope is not continuous at the intersection (i.e. a singularity point) between the Hvorslev envelope and the Mohr-Coulomb envelope. Such a discontinuity in the slope means that the strength cannot be defined at this singular point when, for example, Mohr circles are adopted to interpret the strength of soils. This problem will be discussed in detail in the next section.

In this paper, Hermite interpolation is employed to smooth the transition between the Hvorslev envelope and the zero-tension line as well as the transition between the Hvorslev envelope and the critical state line without additional parameter. The proposed smoothed Hvorslev envelope, which is referred to as Hermite-Hvorslev envelope, will be used to replace the straight Hvorslev envelope which was employed in the original UH model. The UH model revised with the Hermite-Hvorslev envelope will be compared with the original UH model, the UH model with a parabolic Hvorslev envelope and the piecewise Hvorslev envelope. The revised UH model with the Hermite-Hvorslev envelope can well predict the mechanical behaviors of normally consolidated and overconsolidated soils using the same parameters in the modified Cam-Clay model. Finally, drained and undrained triaxial test results from the literature are used to validate the revised UH model with the Hermite-Hvorslev envelope.

2. Hvorslev envelope and strength singularity

In geometry, an 'envelope' of a family of curves in the plane is defined as a curve that is tangent to each member of the family at some points. The Hvorslev envelope is an envelope of a series of Mohr circles at the peak condition for overconsolidated soils and was initially proposed based on the regression of the results from direct shear tests. In addition, as shown in Fig. 1, the Hvorslev envelope is usually associated with the Mohr-Coulomb strength envelope to describe continuous change in the shear strength (τ) for the entire range of the OCRs. It is commonly assumed that the Hvorslev envelope is a straight line with a smaller slope compared with the Mohr-Coulomb envelope (see Fig. 1). Therefore, the Mohr

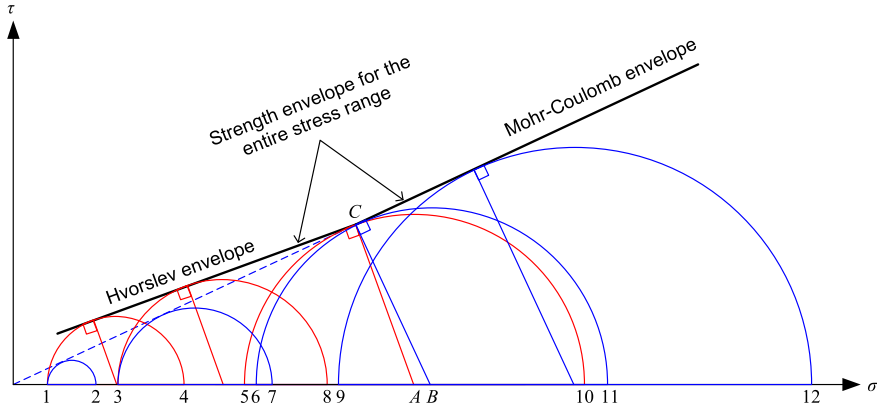

Fig. 1. Interpreting shear strength using Mohr circles, the straight Hvorslev envelope and the Mohr-Coulomb envelope.

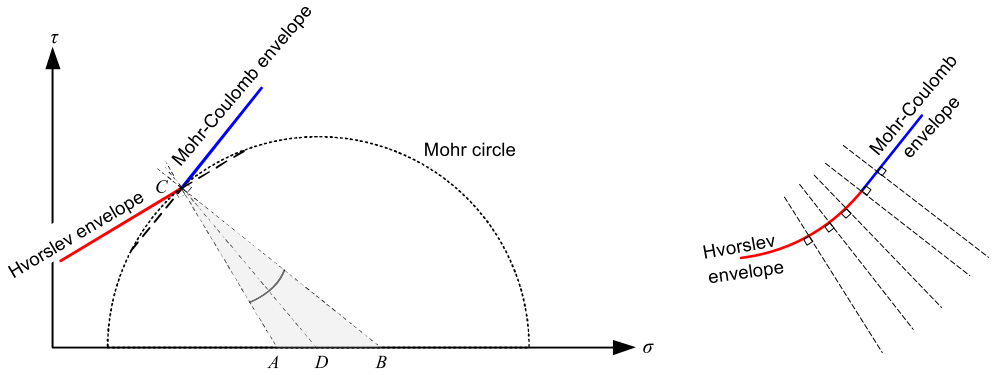

Fig. 2. Unsmoothed transition and smoothed transition between the Hvorslev envelope and the Mohr-Coulomb envelope.

circle tangent to the Hvorslev envelope is larger than the circle tangent to the Mohr-Coulomb envelope if the initial confining stress (σ) is the same (such as the Mohr circle 1–4 versus the Mohr circle 1–2 and the Mohr circle 3–8 versus the Mohr circle 3–7 in Fig. 1). The difference in the shear strengths represented by the Hvorslev envelope and the Mohr-Coulomb envelope decreases with an increase in the initial confining stress (for example, the radius ratio between the Mohr circles 3–8 and 3–7 is larger than that between the Mohr circles 1–4 and 1–2 in Fig. 1). When soil is normally consolidated, the Mohr circle can only be tangent to the Mohr-Coulomb envelope, and the strength is governed by the Mohr-Coulomb envelope only (see the Mohr circle 9–12 in Fig. 1).

However, such a piecewise strength envelope combining straight Hvorslev envelope and Mohr-Coulomb envelope cannot be used for a specific stress range between points *A* and *B*. Point *A* is the center of the Mohr circle that is tangent to the straight Hvorslev envelope at point *C* (the intersecting point between the Hvorslev envelope and the Mohr-Coulomb envelope). Point *B* is the center of the Mohr circle that is tangent to the Mohr-Coulomb envelope at point *C*. All Mohr circles with centers at the left of point *A* (such as Mohr circles 1–4, 3–8 and 5–10 in Fig. 1) have tangent points on the Hvorslev envelope. All Mohr circles with centers at the right of point *B* (such as Mohr circles 6–11 and 9–12 in Fig. 1) have tangent points on the Mohr-Coulomb envelope. However, in terms of an arbitrary Mohr circle with its center located between points *A* and *B* (i.e. point *D* in Fig. 2a), neither the Mohr-Coulomb line nor the Hvorslev line can be used as the strength envelope of this Mohr circle because neither of these two lines is tangent to it. Therefore, such a piecewise strength envelope cannot be applied to the entire stress range because of the unsmoothed transition (i.e. singularity point *C*) between the Hvorslev and the Mohr-Coulomb envelopes. Furthermore, such a piecewise strength envelope mismatches with the definition of 'envelope' in geometry because this piecewise line is not tangent to each member of the family (i.e. each Mohr circle at failure) at some points.

This problem can be solved (see Fig. 2b) if the transition between the Hvorslev envelope and the Mohr-Coulomb line can be smoothed (i.e. the first-order derivative of the entire envelope is continuous). Furthermore, for an overconsolidated soil, if all the Mohr circles at failure with different confining pressures can be determined experimentally, the envelope tangent to these Mohr circles must be a smooth curve theoretically and it is unreasonable that there is a singularity point on the strength envelope.

In addition, the unsmoothed transition between the Hvorslev envelope and the Mohr-Coulomb envelope can also result in computational difficulties due to the gradient discontinuity at the singularity point when the piecewise strength envelope is used as the yield function. With respect to normally consolidated soils, the gradient discontinuity for the singularity points at both the edges and the tip of the hexagonal pyramid (i.e. the Mohr-Coulomb strength envelope) has been discussed by Sloan and Booker (1986) and Abbo and Sloan (1995). From a computational point of view, all of these singularity points should be removed by a mathematical method to ensure that the strength envelope is smooth everywhere. However, in terms of overconsolidated soils, the Mohr-Coulomb envelope will be replaced by the piecewise strength envelope, consisting of the Mohr-Coulomb and the Hvorslev envelopes. Such a replacement will introduce another singularity point (e.g. singularity point *C* in Fig. 2a), which should be removed as well.

In summary, to meet the physical, geometrical and numerical requirements, the strength envelope for normally consolidated and overconsolidated soils should be continuous and smooth for the entire stress range.

3. Smoothed Hvorslev envelope

To produce a Hvorslev envelope (q_{HV}) that can smoothly join into the Mohr-Coulomb envelope at the intersecting point (p_{int}), the following four conditions should be met:

$$\left.\begin{array}{l} p = 0,\ q_{HV} = 0 \\ p = 0,\ q'_{HV} = 3 \\ p = p_{int},\ q_{HV} = Mp_{int} \\ p = p_{int},\ q'_{HV} = M \end{array}\right\} \tag{1}$$

where p is the effective mean stress; q'_{HV} stands for the first-order derivative of q_{HV} towards p; M is the slope of the critical state line, which is $6\sin\phi/(3-\sin\phi)$ if the Mohr-Coulomb criterion is employed, and the Lode's angle is $-30°$.

Hermite interpolation is employed to construct the Hvorslev envelope that meets the four boundary conditions in Eq. (1). In general, Hermite interpolation (H) towards $n+1$ data points (each point contains two conditions) can be written as

$$H(x) = \sum_{i=0}^{n}[y_i\alpha_i(x) + m_i\beta_i(x)] \tag{2}$$

where y_i is equal to $H(x_i)$ and m_i is equal to $H'(x_i)$. α_i and β_i are two Hermite basis functions as follows:

$$\left.\begin{array}{l} \alpha_i(x) = [1 - 2(x - x_i)l'_i(x)]l_i^2(x) \\ \beta_i(x) = (x - x_i)l_i^2(x) \end{array}\right\} \tag{3}$$

Table 1
Basis functions and related parameters for Hermite interpolation.

Data point	Functions and parameters
The first data point ($i = 0$)	$x_0 = 0$, $y_0 = 0$, $m_0 = 3$ $l_0 = (p-p_{int})/p_{int}$ $\alpha_0=(1+2p/p_{int})\,(p/p_{int}-1)^2$ $\beta_0 = p\,(p/p_{int}-1)^2$
The second data point ($i = 1$)	$x_1 = p_{int}$, $y_1 = Mp_{int}$, $m_1 = M$ $l_1 = p/p_{int}$ $\alpha_1= (-2p/p_{int}-1)\,(p/p_{int})^2$ $\beta_1 = (p-p_{int})\,(p/p_{int})^2$

where $l_i(x)$ is the Lagrange basis polynomial function, $l'_i(x)$ is the first-order derivative of $l_i(x)$; and x_i is the value of x at the i-th data point. The first two conditions in Eq. (1) are related to the first data point ($i = 0$), and the last two conditions in Eq. (1) are related to the second data point ($i = 1$). Substituting Eq. (1) into Eq. (2) and replacing x by p, we have the basis functions and the related parameters for Hermite interpolation, as shown in Table 1.

Therefore, the smoothed Hvorslev envelope by Hermite interpolation, which is also referred to as Hermite-Hvorslev envelope, can be written as

$$q_{HV} = \frac{p^3}{p_{int}^2}(3-M) - \frac{2p^2}{p_{int}}(3-M) + 3p \tag{4}$$

Eq. (4) is illustrated in Fig. 3, where the parabolic Hvorslev envelope proposed by Yao et al. (2012) is plotted for comparison purposes. Fig. 3 shows that the Hermite-Hvorslev envelope can realize the smoothed transition between the Hvorslev envelope and the critical state line. The combination of the Hermite-Hvorslev envelope and the Mohr-Coulomb envelope can result in a well-defined strength envelope for the entire range of OCR and meets the geometrical requirements for defining an 'envelope'.

4. Constitutive equations for UH model

Based on the straight Hvorslev envelope, Yao et al. (2009) developed a simple but robust constitutive model for both normally consolidated and overconsolidated soils (i.e. the original UH model) to reproduce the mechanical behaviors in the isotropic and triaxial states, such as inelastic deformation in reloading, peak strength, shear-dilation, and strain-softening. Some basic concepts and assumptions in the original UH model are briefly reviewed here.

4.1. Current and reference yield surfaces

In the original UH model, an ellipse is adopted as the current yield surface following the modified Cam-Clay model (see Fig. 4, solid ellipse OC). With respect to the current yield surface, the UH parameter (H) is adopted to replace the plastic volumetric strain (ε_v^p) that is used as the hardening parameter in the modified Cam-Clay model. The current yield surface and its hardening law are presented as follows:

$$\left.\begin{aligned} &p + \frac{q^2}{pM^2} - p_x = 0 \quad \text{(Current yield surface)} \\ &p_x = p_{x0}\exp\left(\int \frac{1+e}{\lambda-\kappa}\mathrm{d}H\right) \quad \text{(Hardening law)} \end{aligned}\right\} \tag{5}$$

where q is the deviatoric stress, and $q = \eta p$, where η is the stress ratio; p_x is the cross point between the current yield surface and the p-axis; p_{x0} is the equivalent initial effective mean stress (i.e. $p_{x0} = p_0 + q_0^2/(M^2\,p_0)$, where p_0 and q_0 are the initial mean stress and initial deviatoric stress, respectively); e is the void ratio; κ and λ are the elastic unloading index and elastoplastic compression index for saturated soils, respectively; M is the stress ratio at the critical state; and H is the UH parameter proposed by Yao et al. (2007, 2008b, 2009), which can be written as

$$H = \int \mathrm{d}H = \int \frac{M_f^4 - \eta^4}{M^4 - \eta^4}\mathrm{d}\varepsilon_v^p \tag{6}$$

where M_f is the potential peak stress ratio and can be determined based on the straight Hvorslev envelope (or other functions of Hvorslev envelope, which will be discussed in the following section). The initial size of the current yield surface is determined by the value of p_{x0} (see the initial ellipse OC_0 in Fig. 4). During a triaxial loading, e.g. conventional triaxial compression (CTC, see stress path C_0A in Fig. 4), the current state point moves from C_0 to point A, and the current yield surface expands from OC_0 to OC. The increments of the UH parameter ($\mathrm{d}H$) and the plastic volumetric strain ($\mathrm{d}\varepsilon_v^p$) can be calculated from Eqs. (5) and (6) when the yield surface expands from OC_0 to OC. Conversely, the current yield surface can be

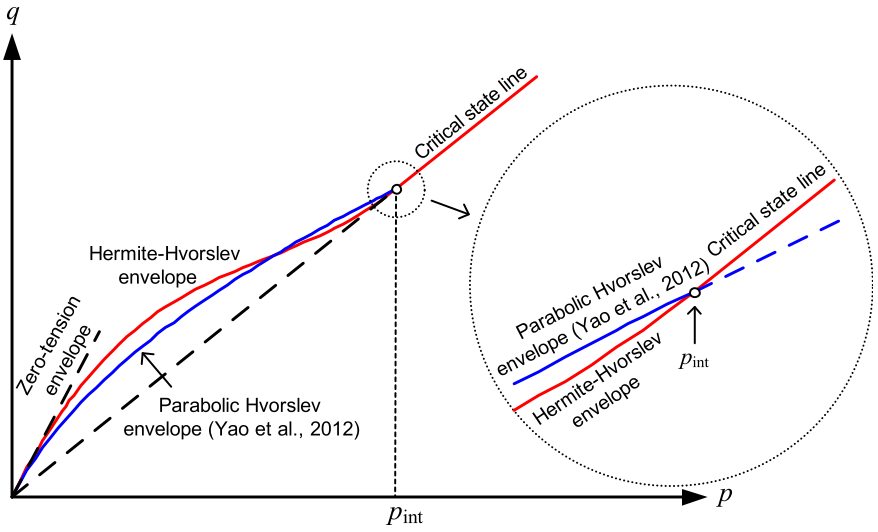

Fig. 3. Schematic diagram of the Hermite-Hvorslev envelope and the parabolic Hvorslev envelope.

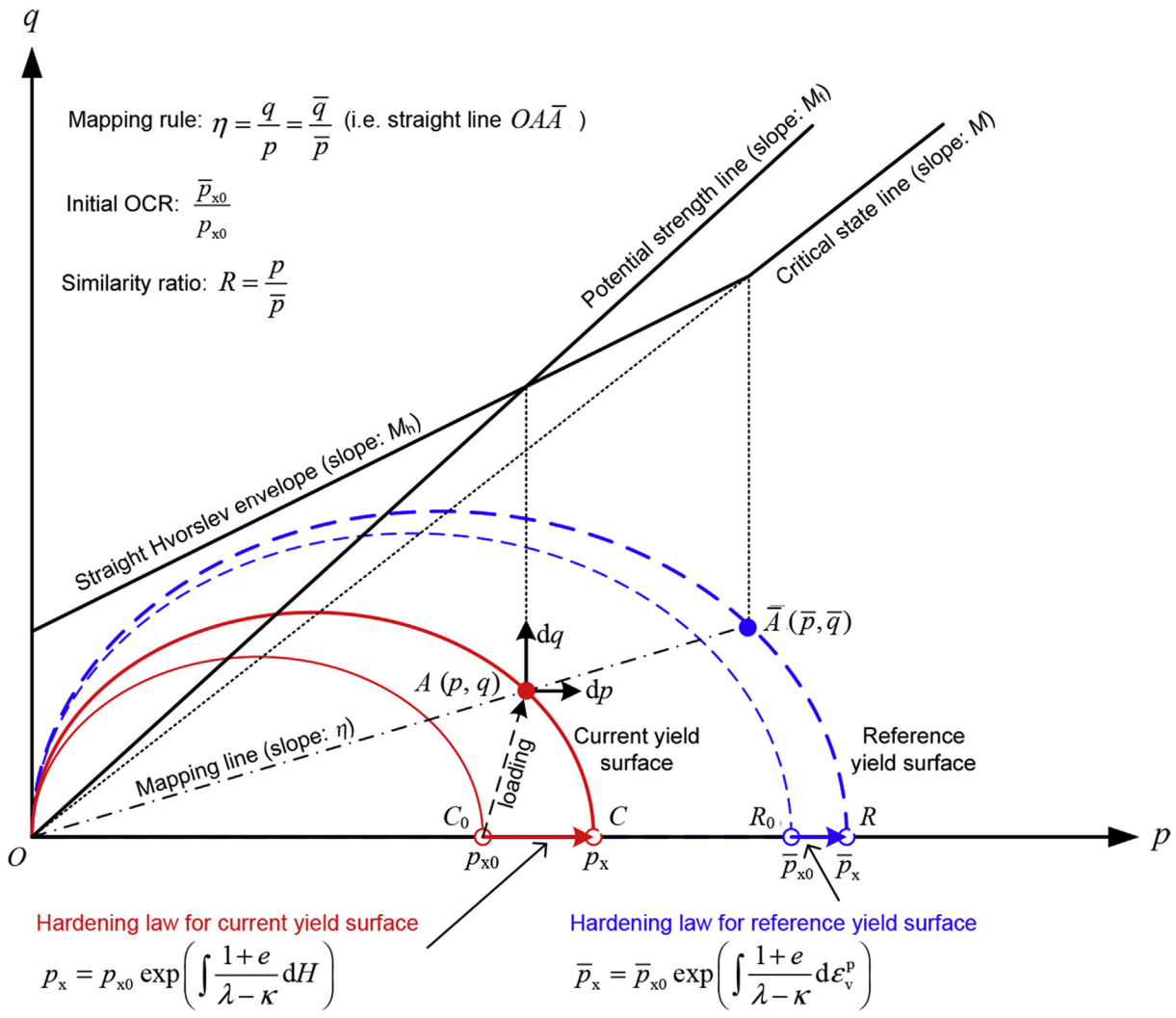

Fig. 4. Schematic diagram of the original UH model.

determined according to Eqs. (5) and (6) with a given increment of the plastic volumetric strain in strain-controlled loading.

In addition to the current yield surface, the reference yield surface (see Fig. 4, dash ellipse *OR*), which is completely identical to the yield surface in the modified Cam-Clay model, is adopted to consider the effect of the stress history and further determine the evolution of M_f (see the following section). The reference yield surface and its hardening law can be written as

$$\left.\begin{aligned} \overline{f} &= \overline{p} + \frac{\overline{q}^2}{\overline{p}M^2} - \overline{p}_x = 0 \quad \text{(Current yield surface)} \\ \overline{p}_x &= \overline{p}_{x0}\exp\left(\int \frac{1+e}{\lambda-\kappa} d\varepsilon_v^p\right) \quad \text{(Hardening law)} \end{aligned}\right\} \tag{7}$$

where $\overline{p}$ and $\overline{q}$ are the reference mean stress and the reference deviatoric stress, respectively; $\overline{p}_x$ is the cross point between the reference yield surface and the *p*-axis; and $\overline{p}_{x0}$ is the isotropic preconsolidation pressure. The initial size of the reference yield surface is specified by the value of $\overline{p}_{x0}$ (see the initial ellipse OR_0 in Fig. 4). The expansion of the reference yield surface is controlled by the plastic volumetric strain. The plastic volumetric strain produced when the current yield surface expands from OC_0 to *OC* leads to the expansion of the reference yield surface from OR_0 to *OR* (see Fig. 4). It is noted that the expansion velocity difference between the current and the reference yield surfaces is controlled by the value of the term $(M_f^4 - \eta^4)/(M^4 - \eta^4)$.

4.2. Mapping rule and similarity ratio

The reference yield surface can be determined by $\overline{p}_{x0}$ and the term related to the plastic volumetric strain (i.e. $\int[(1+e)/(\lambda-\kappa)]d\varepsilon_v^p$). A mapping rule is still required to find the reference point (see point $\overline{A}$ in Fig. 4) on the reference yield surface to specify $\overline{p}$ and $\overline{q}$. A geometrical mapping rule between the reference and the current stress points is assumed as

$$\eta = q/p = \overline{q}/\overline{p} \tag{8}$$

Eq. (8) indicates that the stress ratio of the current stress point is always equal to that of the reference point. Geometrically, the reference point is defined as the cross point between the reference yield surface, a straight line passing through the origin (i.e. point *O*) and the current state point (i.e. point *A*). Hashiguchi (1989) first introduced the similarity ratio between a sub-loading surface and a yield surface as a state variable in the unconventional plasticity model. Asaoka et al. (2000) employed the similarity ratio between a sub-loading surface and a super-loading surface as a state variable

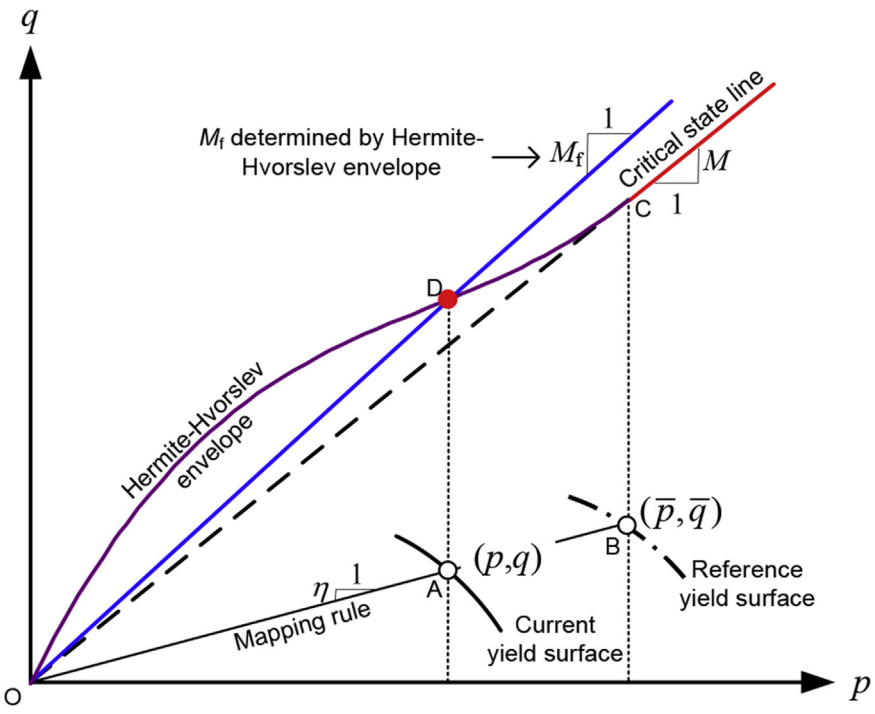

Fig. 5. Determining the potential peak stress ratio using the Hermite-Hvorslev envelope.

to quantify the evolution of the degree of overconsolidation during triaxial shearing. Following Asaoka et al. (2000), the similarity ratio, i.e. the ratio between the current mean stress (p) and the reference mean stress ($\bar{p}$), is adopted as a state variable (R):

$$R = p/\bar{p} \tag{9}$$

where $\bar{p}$ can be solved from Eq. (7), and it can be written as

$$\bar{p} = \bar{p}_{x0}\frac{M^2}{\eta^2+M^2}\exp\left(\int\frac{1+e}{\lambda-\kappa}\mathrm{d}\varepsilon_v^p\right)$$

4.3. Flow rule and elastic responses

The flow rule similar to that in the modified Cam-Clay model is employed here:

$$\frac{\mathrm{d}\varepsilon_d^p}{\mathrm{d}\varepsilon_v^p} = \frac{2\eta}{M^2-\eta^2} \tag{10}$$

where $\mathrm{d}\varepsilon_d^p$ is the plastic deviatoric strain. The elastic volumetric strain and elastic deviatoric strain are defined as follows:

$$\left.\begin{aligned}\mathrm{d}\varepsilon_v^e &= \frac{\kappa}{1+e}\frac{\mathrm{d}p}{p}\\ \mathrm{d}\varepsilon_d^e &= \frac{2(1+\nu)}{9(1-2\nu)}\frac{\kappa}{1+e}\frac{\mathrm{d}q}{p}\end{aligned}\right\} \tag{11}$$

where ν is the Poisson's ratio, the value of which is usually estimated between 0 and 0.4.

5. Determining potential peak stress ratio by Hermite-Hvorslev envelope

The concept of potential peak stress ratio (M_f) is of critical importance in the original UH model. M_f represents the potential peak shear strength for normally consolidated and overconsolidated soils and varies according to the evolution of the similarity ratio (R) during shearing. It can be estimated from the strength envelope for normally consolidated and overconsolidated soils. In general, M_f can be written as

$$M_f = \frac{q_{HV}\big|_{p_{int}=\bar{p}}}{p} \tag{12}$$

Eq. (12) is a general equation to calculate the value of M_f. $q_{HV}\big|_{p_{int}=\bar{p}}$ is the deviatoric stress which can be determined from the Hvorslev envelope when the mean stress of intersecting point is set to the reference mean stress. In the revised UH model, the proposed Hermite-Hvorslev envelope is adopted to replace the straight Hvorslev envelope in the original UH model (see Fig. 4). Substituting the proposed Hermite-Hvorslev envelope (i.e. Eq. (4)) into Eq. (12) and letting $p_{int} = \bar{p}$, we have

$$M_f = \frac{p^2}{\bar{p}^2}(3-M) - \frac{2p}{\bar{p}}(3-M) + 3 \tag{13}$$

The process of determining M_f mentioned above can be interpreted through the following geometrical method. For a given current stress state (i.e. current stress point A in Fig. 5), we can find its corresponding reference stress point (point B), which is an intersection between the reference yield surface and the straight line (i.e. mapping rule) passing through both the origin (point O) and the current stress point (point A). According to the location of the reference stress point (point B), the intersecting point (point C) between the Hermite-Hvorslev envelope and the critical state line can be determined (i.e. $p_{int} = \bar{p}$). Once the intersecting point is fixed, the location of the Hermite-Hvorslev envelope can be determined, and the potential peak stress ratio (the stress ratio represented by the point D, i.e. M_f) can be read from the Hermite-Hvorslev envelope according to the current mean stress (mathematically represented by Eq. (13)).

Substituting Eq. (9) into Eq. (13) yields

$$M_f = R^2(3-M) - 2R(3-M) + 3 \tag{14}$$

Eq. (14) indicates that the potential peak stress ratio based on the Hermite-Hvorslev envelope can be written as a function of the critical state stress ratio (M) and the similarity ratio (R), which does not involve any additional material parameters.

In addition to the Hermite-Hvorslev envelope, the other expressions of the Hvorslev envelope can also be used to specify the equation of M_f. For example, in the original UH model (Yao et al., 2009), the Hvorslev envelope was assumed to be a straight line (see Fig. 4) with the slope equal to M_h:

$$q_{HV} = (M - M_h)(p_{int} - p) + Mp \tag{15}$$

The corresponding potential peak stress ratio can be written as

$$M_f = (1/R - 1)(M - M_h) + M \tag{16}$$

Eq. (16) indicates that the potential peak stress ratio based on the straight Hvorslev envelope requires an additional parameter (i.e. the slope of the straight Hvorslev envelope, M_h) in addition to the critical state stress ratio (M).

To satisfy the restriction that the stress ratio should always be less than three in the p-q plane, a complicated parabolic function (Yao et al., 2012) was adopted to represent the Hvorslev envelope as

$$q_{HV} = \sqrt{\frac{3M^2 p_{int}}{3-M}\left[p + \frac{M^2 p_{int}}{12(3-M)}\right]} - \frac{M^2 p_{int}}{2(3-M)} \tag{17}$$

The corresponding potential peak stress ratio can be written as

$$M_f = \sqrt{\frac{3M^2}{(3-M)R}\left[1 + \frac{M^2}{12R(3-M)}\right]} - \frac{M^2}{2R(3-M)} \tag{18}$$

It is noted that Eq. (18) is based on a subjective assumption. It is assumed that the Hvorslev envelope must be expressed by an ad hoc parabolic function without any justification.

A piecewise Hvorslev envelope (Yao and Zhou, 2013) was suggested to remove the subjective assumption (i.e. the Hvorslev envelope must be expressed by a parabolic function) but still satisfy the restriction:

$$q_{HV} = \begin{cases} 3p & \left(p \le \dfrac{M - M_h}{3 - M_h} p_{int}\right) \\ (M - M_h)(p_{int} - p) + Mp & \left(p > \dfrac{M - M_h}{3 - M_h} p_{int}\right) \end{cases} \tag{19}$$

The corresponding potential peak stress ratio can be written as

$$M_f = \begin{cases} 3 & \left(R \le \dfrac{M - M_h}{3 - M_h}\right) \\ \left(\dfrac{1}{R} - 1\right)(M - M_h) + M & \left(R > \dfrac{M - M_h}{3 - M_h}\right) \end{cases} \tag{20}$$

The advantages and limitations of the four equations (i.e. Eqs. (4), (15), (17) and (19)) representing the Hvorslev envelope are compared in Table 2. Table 2 shows that all the equations for the Hvorslev envelope, except the straight line, take into account the restriction on the maximum stress ratio in the p-q plane. Only the parabolic Hvorslev envelope assumes that the shape of the Hvorslev envelope is a parabolic curve beforehand. The straight Hvorslev envelope and the piecewise Hvorslev envelope are more flexible when incorporating experimental data because both of them employ an additional parameter (i.e. M_h). The parabolic Hvorslev envelope and the Hermite-Hvorslev envelope are more practical and applicable in practice, especially when the test data of the peak strength are unavailable. Furthermore, only the Hermite-Hvorslev envelope is smooth for the entire stress range and meets the geometrical definition of an 'envelope', which is the most important in the proposed equation.

As illustrated above, all four different Hvorslev envelopes listed above can be used to specify the value of M_f in Eq. (12). Eqs. (14), (16), (18) and (20) represent the expressions of M_f based on the Hermite-Hvorslev envelope, the straight Hvorslev envelope, the parabolic Hvorslev envelope and the piecewise Hvorslev envelope, respectively. The comparisons among these expressions of M_f show that in addition to the material constants (such as M and M_h if required), M_f is fully governed by the similarity ratio R. Because the similarity ratio (R) changes during isotropic and non-isotropic compressions, the value of M_f varies accordingly during the entire loading process. For example, at the beginning of triaxial compression for overconsolidated soil ($OCR > 1$), M_f is at its highest value because the value of R is the lowest at the initial state for loading conditions. The highest value of M_f at the initial state can only be regarded as a 'potential' strength, corresponding to the initial R. Along with the increase in the deviatoric stress (i.e. the increase in the stress ratio), R keeps increasing. The increase in R leads to a decrease in M_f, which means that the potential strength of the soil keeps decreasing during shearing. Once the stress ratio (η) equals the potential strength (M_f), the potential strength becomes the real peak strength of the soil. After the peak strength point, M_f keeps decreasing until its value reaches M (critical state). Specially, $M_f = M$ if $R = 1$ (i.e. the soil is normally consolidated or at the critical state).

Comparing the four equations of M_f (i.e. Eqs. (14), (16), (18) and (20)) indicates that Eqs. (16) and (18) will be undefined when R is equal to zero (i.e. OCR is infinite). In addition, it is noted that if either M_f based on the parabolic Hvorslev envelope (i.e. Eq. (18)) or M_f based on the Hermite-Hvorslev envelope (i.e. Eq. (14)) is adopted, the proposed UH model will not introduce any additional parameters compared with the modified Cam-Clay model, but can be used for normally consolidated and overconsolidated soils. However, as stated before, only the combination of the Hermite-Hvorslev envelope and the Mohr-Coulomb envelope can meet the physical, geometrical and numerical requirements of a strength envelope for normally consolidated and overconsolidated soils. Therefore, the Hermite-Hvorslev envelope is preferably employed to estimate the potential peak stress ratio in the UH model.

Table 2
Comparison of four different equations for the Hvorslev envelope.

Hvorslev envelope	Restriction on the maximum stress ratio	Subjective assumption	Flexibility	Additional parameter	Smoothed transition	Geometrical requirement
Straight Hvorslev envelope (Eq. (15))	×	√	√	×	×	×
Parabolic Hvorslev envelope (Eq. (17))	√	×	×	√	×	×
Piecewise Hvorslev envelope (Eq. (19))	√	√	√	×	×	×
Hermite-Hvorslev envelope (Eq. (4))	√	√	×	√	√	√

Note: '√' denotes advantageous and '×' denotes disadvantageous.

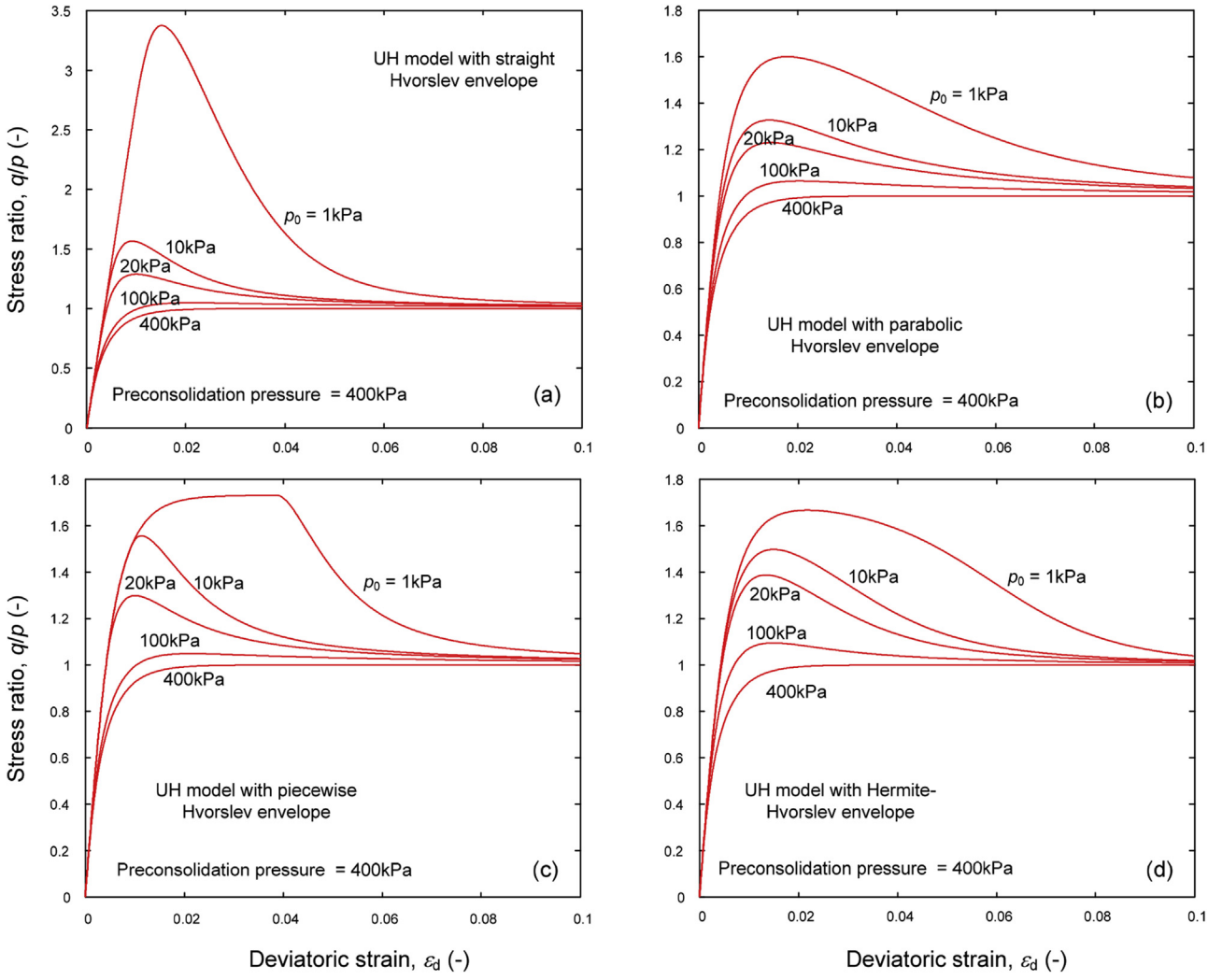

Fig. 6. Stress–strain relationships predicted by the UH models with four different Hvorslev envelopes for various OCRs.

Table 3
Parameters for the UH models with different Hvorslev envelopes.

UH model	M	λ	κ	ν	M_h
UH model with a straight Hvorslev envelope (i.e. original UH model)	1	0.1	0.01	0.3	0.8
UH model with a parabolic Hvorslev envelope	1	0.1	0.01	0.3	N/N
UH model with a piecewise Hvorslev envelope	1	0.1	0.01	0.3	0.8
UH model with the Hermite-Hvorslev envelope (i.e. revised UH model)	1	0.1	0.01	0.3	N/N

Note: Not denotes 'not necessary'.

6. Comparison of UH models with different Hvorslev envelopes

Four different equations (i.e. Eqs. (14), (16), (18) and (20)) for the potential peak stress ratio (M_f) are embedded in the UH model, and the predictions are presented in Fig. 6. The model parameters for the hypothetical soil are listed in Table 3. For clays, M_h is usually 0.5M–0.9M (Mita et al., 2004), and this range is used to estimate M_h (M_h is assumed as 0.8M here).

The hypothetical soil is first isotropically sampled under a preconsolidation pressure of 400 kPa and then unloaded to 400 kPa, 100 kPa, 20 kPa, 10 kPa and 1 kPa to produce different OCRs of specimens (OCR = 1, 4, 20, 40 and 400, respectively). The hypothetical specimens are triaxially compressed in undrained conditions. Four UH models are employed to simulate the responses of the five soil specimens mentioned above. Fig. 6a shows the stress–strain curves predicted by the UH model with a straight Hvorslev envelope (i.e. original UH model). Fig. 6b shows the stress–strain curves predicted by the UH model with a parabolic Hvorslev envelope. The stress–strain curves predicted by the UH model with a piecewise Hvorslev envelope and a Hermite-Hvorslev envelope (i.e. revised UH model) are presented in Fig. 6c and d, respectively.

The comparison shown in Fig. 6 indicates that:

(1) The UH models with four different Hvorslev envelopes can predict the peak strength and post-peak softening, at least qualitatively, caused by overconsolidation.
(2) The UH models with four different Hvorslev envelopes produce similar stress–strain curves when the OCR is relatively small.
(3) When the OCR is very high (e.g. OCR = 400), the UH model with the straight Hvorslev envelope will overestimate the peak strength (i.e. predicted stress ratio may go beyond three), and the UH model with a piecewise Hvorslev envelope will predict a peak strength plateau followed by softening. Compared with the UH model with a parabolic Hvorslev envelope, the UH model with a Hermite-Hvorslev envelope will

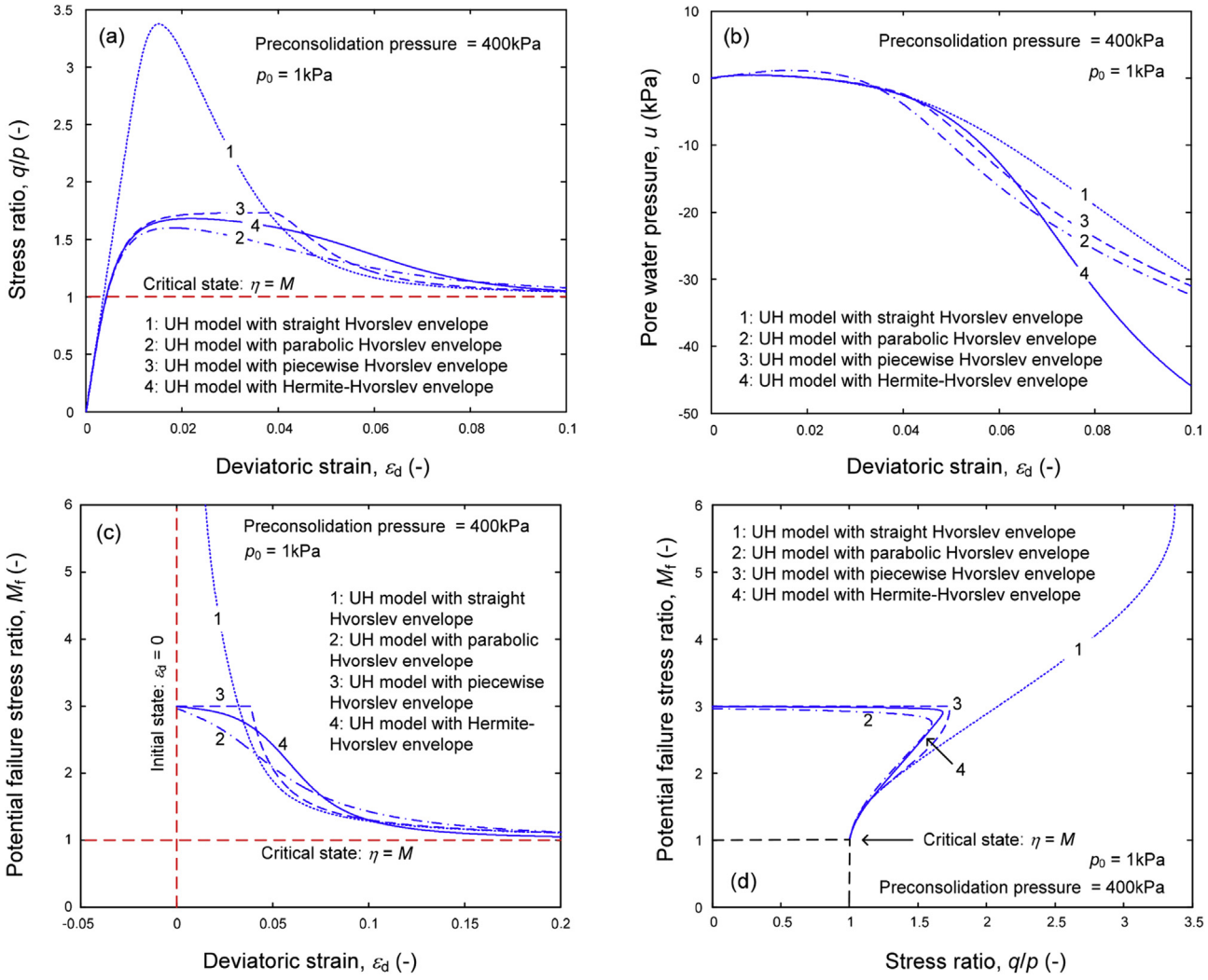

Fig. 7. Stress–strain relationships and pore water pressure change predicted by the UH models with four different Hvorslev envelopes for a very high OCR value.

predict a higher stress ratio (i.e. stiffer stress–strain curve), which will lead to better agreement with the test results. As remarked in Yao et al. (2012), "*the UH model (with parabolic Hvorslev envelope) tends to give softer responses than the measured ones*", and "*to achieve more accurate predictions, plausible improvement can be made by modifying the UH parameter to obtain a stiffer soil response at high OCR values*".

(4) Compared with the UH model with a parabolic Hvorslev envelope, the stress–strain curves predicted by the UH model with a Hermite-Hvorslev envelope exhibit better convergence when the deviatoric strain (ε_d) goes beyond 0.1.

Given that the differences among UH models with different Hvorslev envelopes are more distinct at a high OCR value, the stress–strain curves (see Fig. 7a) and pore water pressures (see Fig. 7b) predicted by the four UH models are compared with each other when the OCR value is 400. The UH model with a Hermite-Hvorslev envelope predicts a larger negative pore water pressure than the UH models with the other three Hvorslev envelopes in undrained conditions. In other words, in drained conditions, the UH model with a Hermite-Hvorslev envelope will predict more distinct shear-induced dilatancy, which leads to a better simulation of the measured results (see the following section). In addition, the evolution of the potential peak stress ratio (M_f) along with the increase in the deviatoric strain (ε_d) is shown in Fig. 7c. The relationship between the potential peak stress ratio (M_f) and the stress ratio (η) during shearing is presented in Fig. 7d. Except the UH model with a straight Hvorslev envelope, in which the potential peak stress ratio may reach an extremely high value at the beginning of the shearing, the UH model with the other Hvorslev envelopes (i.e. parabolic, piecewise and Hermite) can limit the stress ratio between three and the critical state stress ratio (M). The evolution curves (see Fig. 7c and d) of the potential peak stress ratio governed by the Hermite-Hvorslev envelope are between the M_f curve controlled by the piecewise Hvorslev envelope and that by the parabolic Hvorslev envelope.

7. Experimental validations

The performances of the UH model revised by the smoothed Hvorslev envelope (i.e. Hermite-Hvorslev envelope) are evaluated by the experimental results published in the literature. Drained and undrained data are included in the experimental validations here.

7.1. Drained triaxial tests on Fujinomori clay

Nakai and Hinokio (2004) conducted a series of drained triaxial compression tests with constant mean stresses (p is constant) on

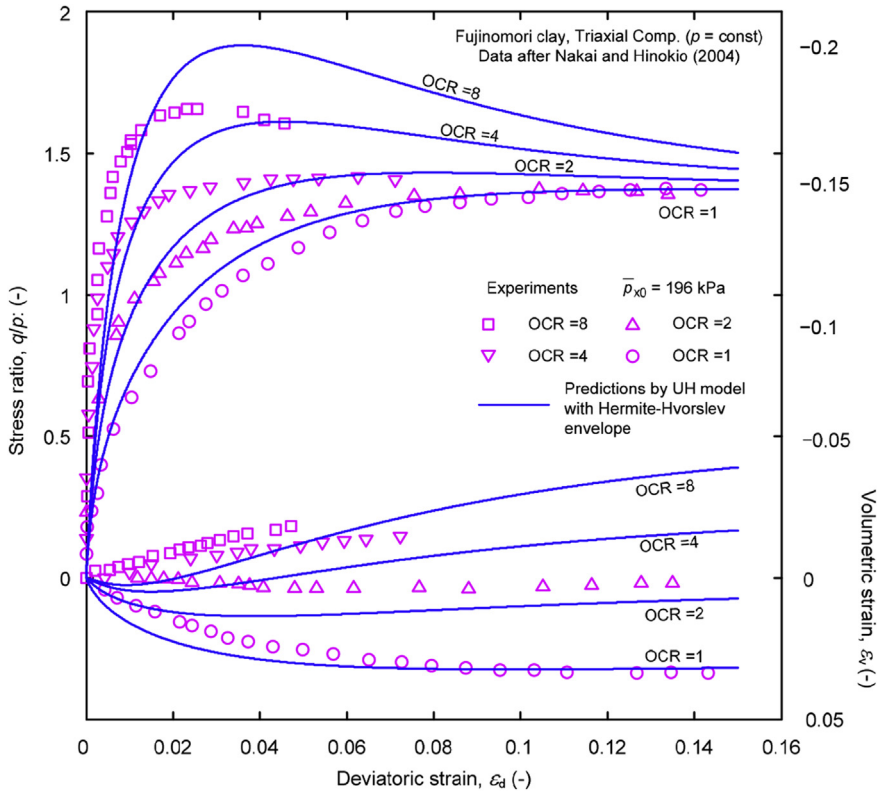

Fig. 8. Measured and predicted stress–strain relationships and volume change for Fujinomori clay with different OCRs in drained conditions (data after Nakai and Hinokio, 2004).

four Fujinomori clay specimens with different OCR values (1, 2, 4 and 8). Four soil specimens were first isotropically preconsolidated to 196 kPa, 392 kPa, 784 kPa and 784 kPa, and then the mean stresses for them were reduced to 196 kPa, 196 kPa, 196 kPa and 98 kPa, respectively, to generate different OCR values (1, 2, 4 and 8). After specimen preparation, these four specimens were triaxially sheared to the peak with constant initial mean stresses (i.e. 196 kPa for $OCR = 1$, 2 and 4, and 98 kPa for $OCR = 8$). The test results (stress–strain relationships as well as the volumetric strain developments during shearing) are replotted in Fig. 8. Because the UH model with a Hermite-Hvorslev envelope does not require any additional material parameters, the model predictions are fully based on the calibrated material parameters presented by Nakai and Hinokio (2004). The material parameters for Fujinomori clay are listed in Table 4, and the model predictions are plotted in Fig. 8 (see prediction curves). According to the comparison, the model predicts the peak strength, post-peak softening and shear-induced dilation of four different clay specimens reasonably well. However, compared with the experimental results, the model prediction shows a softer stress–strain relationship when the deviatoric strain is relatively low, but indicates a higher peak strength. In terms of the volume change, the model prediction underestimates the shear-dilation, especially when the soil specimen is highly overconsolidated.

Table 4
Material parameters for Fujinomori and kaolin clays.

Clay	$\lambda/(1+e_0)$	$\kappa/(1+e_0)$	M	ν
Fujinomori clay (after Nakai and Hinokio, 2004)	0.0508	0.0112	1.36	0.1
Kaolin clay (Dafalias and Herrmann, 1986)	0.0718	0.0256	1.04	0.3

7.2. Undrained triaxial tests on kaolin clay

The performances of the UH model revised by a Hermite-Hvorslev envelope are further evaluated against the experimental results in the undrained conditions. Banerjee and Stipho (1978, 1979) reported a series of undrained triaxial compression tests on normally consolidated and overconsolidated kaolin clays ($OCR = 1$, 1.2, 5, 8 and 12). These experimental data were employed to validate the boundary surface model, and the material parameters (listed in Table 4) were calibrated by Dafalias and Herrmann (1986). Fig. 9 shows the measured and predicted effective stress paths in the plane of the normalized deviatoric stress $(q/\bar{p}_{x0})$ and the normalized effective mean stress $(p/\bar{p}_{x0})$.The comparisons of the measured and predicted relationships between the pore water pressure (u) and the axial strain (ε_1) are illustrated in Fig. 10, and the comparisons of the measured and predicted relationships between the normalized deviatoric stress $(q/\bar{p}_{x0})$and axial strain (ε_1) are illustrated in Fig. 11. The preconsolidation pressures and OCRs for the specimens are indicated in each figure. The comparisons shown in Fig. 9 indicate that the predicted effective stress paths overestimate the measured stiffness for normally and lightly overconsolidated soil specimens (i.e. $OCR = 1$ and 1.2). For heavily overconsolidated soil specimens, such as $OCR = 12$, the predicted effective stress paths underestimate the measured stiffness. However, the prediction curves shown in Fig. 9 match the experimental results reasonably well. Except for the relationship between the normalized deviatoric stress and the axial strain for normally and lightly overconsolidated soil specimens (i.e. $OCR = 1$ and 1.2) shown in Fig. 11, the comparisons between the test data and the prediction curves show that the model predictions agree well with the experimental results. The UH model with a parabolic Hvorslev envelope was also employed to predict these experimental results

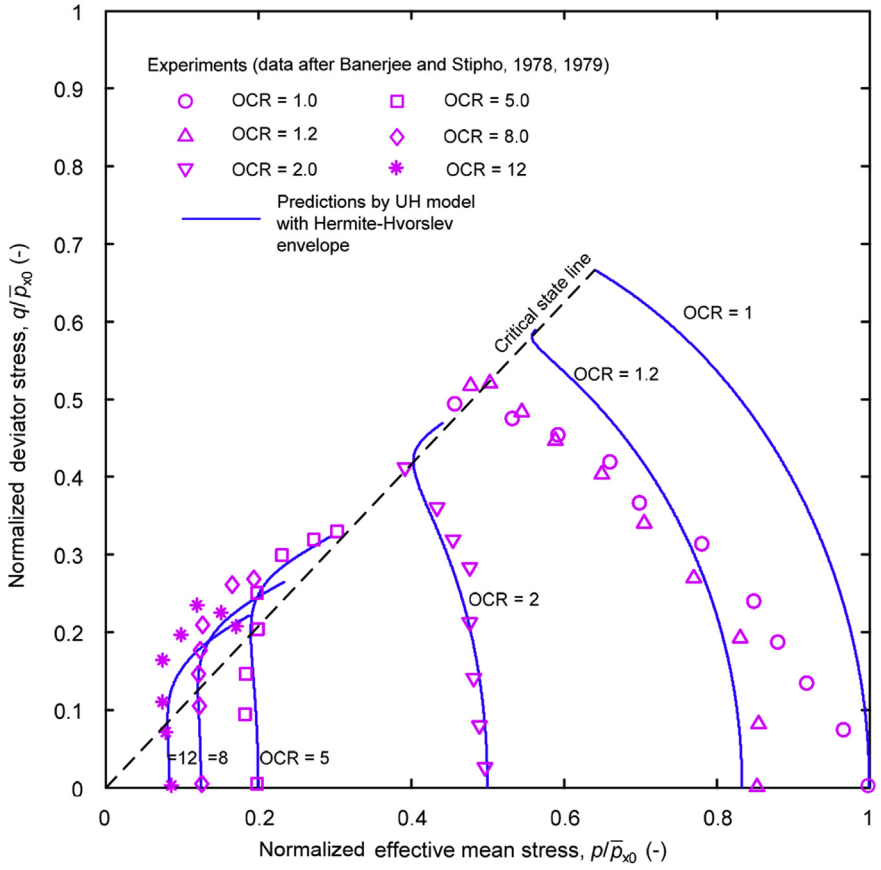

Fig. 9. Measured and predicted effective stress paths for kaolin clay with different OCRs in undrained conditions (data after Banerjee and Stipho, 1978, 1979).

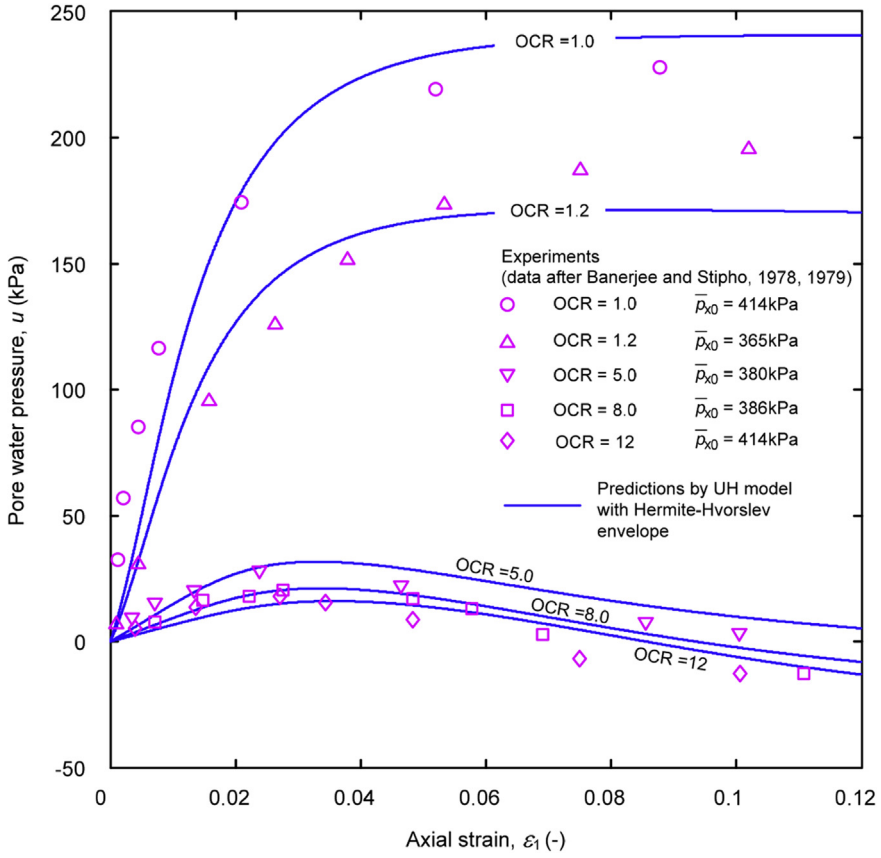

Fig. 10. Measured and predicted pore water pressure changes for kaolin clay with different OCRs in undrained conditions (data after Banerjee and Stipho, 1978, 1979).

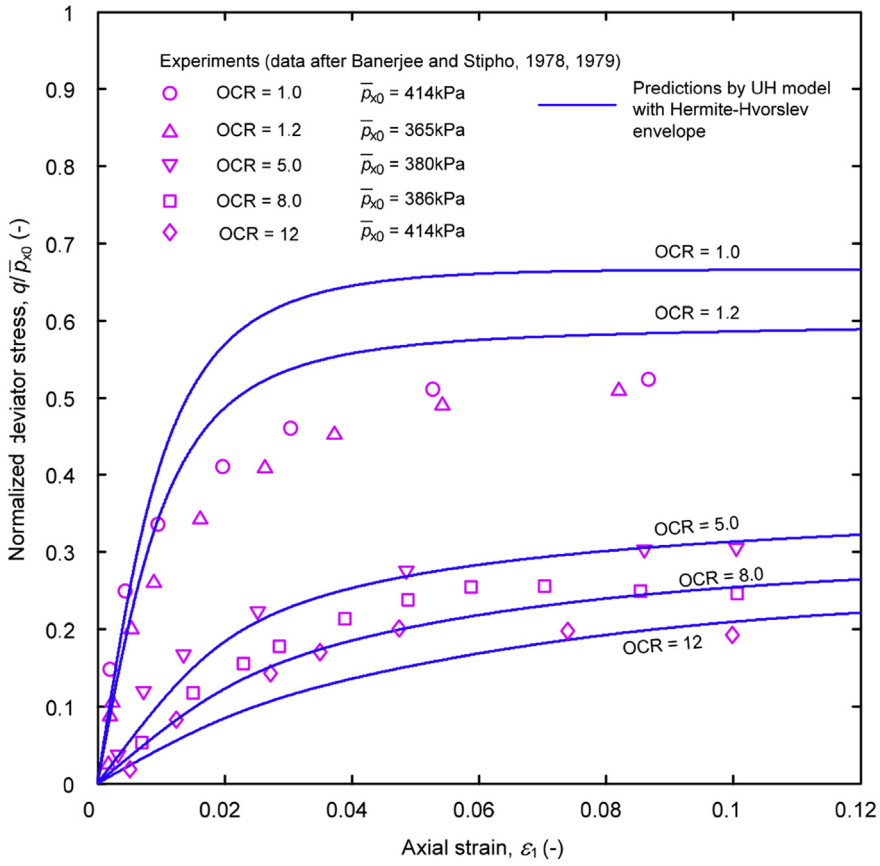

Fig. 11. Measured and predicted stress–strain relationships for kaolin clay with different OCRs in undrained conditions (data after Banerjee and Stipho, 1978, 1979).

(see Fig. 6a, b and d in Yao et al., 2012). Compared with the UH model with a parabolic Hvorslev envelope, the UH model with a Hermite-Hvorslev envelope predicts a higher strength and a larger negative pore water pressure, which makes the predictions closer to the experimental results.

8. Conclusions

A novel and simple equation for the Hvorslev envelope is proposed by the Hermite interpolation method, which is referred to as the Hermite-Hvorslev envelope in this paper. The proposed Hermite-Hvorslev envelope ensures a smoothed transition between the Hvorslev envelope and the zero-tension line as well as a smoothed transition between the Hvorslev envelope and the Mohr-Coulomb envelope. The Hermite-Hvorslev envelope is then integrated into the UH model to specify the potential peak stress ratio (M_f), which is of pivotal importance in the UH model. The UH model revised by the Hermite-Hvorslev envelope, which requires no additional material parameters compared to the modified Cam-Clay model, is employed to predict the overconsolidated soil behavior in the drained and undrained conditions. The performances of the UH model revised by the Hermite-Hvorslev envelope are validated by the comparisons between the measured and predicted soil responses.

Conflict of interest

The authors wish to confirm that there are no known conflicts of interest associated with this publication and there has been no significant financial support for this work that could have influenced its outcome.

Acknowledgement

This study was financially supported by the Australian Research Council DECRA (Grant No. DE130101342) and the National Program on Key Basic Research Project of China (Grant No. 2014CB047006).

References

Abbo AJ, Sloan SW. A smooth hyperbolic approximation to the Mohr-Coulomb yield criterion. Computers & Structures 1995;54(3):427–41.
Asaoka A, Nakano M, Noda T. Superloading yield surface concept for highly structured soil behaviour. Soils and Foundations 2000;40(2):99–110.
Banerjee PK, Stipho AS. Associated and non-associated constitutive relations for undrained behaviour of isotropic soft clays. International Journal for Numerical and Analytical Methods in Geomechanics 1978;2(1):35–56.
Banerjee PK, Stipho AS. An elasto-plastic model for undrained behaviour of heavily overconsolidated clays. International Journal for Numerical and Analytical Methods in Geomechanics 1979;3(1):97–103.
Dafalias Y, Herrmann L. Bounding surface plasticity. II: application to isotropic cohesive soils. Journal of Engineering Mechanics 1986;112(12):1263–91.
Hashiguchi K. Constitutive equations of elastoplastic materials with elastic-plastic transition. Journal of Applied Mechanics 1980;47(2):266–72.
Hashiguchi K. Subloading surface model in unconventional plasticity. International Journal of Soilds and Structures 1989;25(8):917–45.
Ling H, Yue D, Kaliakin V, Themelis N. Anisotropic elastoplastic bounding surface model for cohesive soils. Journal of Engineering Mechanics 2002;128(7):748–58.
Mita KA, Dasari GR, Lo KW. Performance of a three-dimensional Hvorslev-modified Cam clay model for overconsolidated clay. International Journal of Geomechanics 2004;4(4):296–309.
Morvan M, Wong H, Branque D. An unsaturated soil model with minimal number of parameters based on bounding surface plasticity. International Journal for Numerical and Analytical Methods in Geomechanics 2010;34(14):1512–37.
Mrőz Z, Norris VA, Zienkiewicz OC. An anisotropic hardening model for soils and its application to cyclic loading. International Journal for Numerical and Analytical Methods in Geomechanics 1978;2(3):203–21.

Nakai T, Hinokio M. A simple elastoplastic model for normally and overconsolidated soils with unified material parameters. Soils and Foundations 2004;44(2):53–70.
Pender MJ. A model for the behaviour of overconsolidated soil. Geotechnique 1978;28(1):1–25.
Sloan SW, Booker JR. Removal of singularities in Tresca and Mohr-Coulomb yield functions. International Journal for Numerical Methods in Biomedical Engineering 1986;2(2):173–9.
Whittle A, Kavvadas M. Formulation of MIT-E3 constitutive model for overconsolidated clays. Journal of Geotechnical Engineering 1994;120(1):173–98.
Yao Y, Gao Z, Zhao J, Wan Z. Modified UH model: constitutive modeling of overconsolidated clays based on a parabolic Hvorslev envelope. Journal of Geotechnical and Geoenvironmental Engineering 2012;138(7):860–8.
Yao Y, Hou W, Zhou A. Constitutive model for overconsolidated clays. Science in China Series E Technological Sciences 2008a;51(2):179–91.
Yao Y, Hou W, Zhou A. UH model: three-dimensional unified hardening model for overconsolidated clays. Geotechnique 2009;59(5):451–69.
Yao Y, Kong L, Zhou A, Yin J. Time-dependent unified hardening model: three-dimensional elastoviscoplastic constitutive model for clays. Journal of Engineering Mechanics 2015;141(6). https://doi.org/10.1061/(ASCE)EM. 1943-7889.0000885.
Yao Y, Sun D, Matsuoka H. A unified constitutive model for both clay and sand with hardening parameter independent on stress path. Computers and Geotechnics 2008b;35(2):210–22.
Yao Y, Zhou A. Non-isothermal unified hardening model: a thermo-elastoplastic model for clays. Geotechnique 2013;63(15):1328–45.
Yao Y, Zhou A, Lu D. Extended transformed stress space for geomaterials and its application. Journal of Engineering Mechanics 2007;133(10):1115–23.
Zhou A, Sheng D. An advanced hydro-mechanical constitutive model for unsaturated soils with different initial densities. Computers and Geotechnics 2015;63:46–66.